EFFECT OF THERMALLY ACTIVE ZONES AND DIRECTION OF MAGNETIC FIELD ON HYDROMAGNETIC CONVECTION IN AN ENCLOSURE

by

***Sivanandam SIVASANKARAN*[*], *Marimuthu BHUVANESWARI*[1]**

[*]*University College, Sungkyunkwan University, Suwon 440-746, South Korea*

Email: sd.siva@yahoo.com

[1]*Department of Mechanical Engineering, Sungkyunkwan University, Suwon 440-746, South Korea*

The aim of the present numerical study is to investigate the effect of thermally active zones and direction of the external magnetic field on hydromagnetic convection in an enclosure. Nine different relative positions of the thermally active zones are considered. Top and bottom of the enclosure are adiabatic. The governing equations are solved by the finite volume method. The results are obtained for different directions of the external magnetic field, thermally active locations, Hartmann numbers, Grashof numbers and aspect ratios. It is observed that the heat transfer is enhanced for heating location is either at middle or at bottom of the hot wall while the cooling location is either at top or at middle of the cold wall. The flow field is altered when changing the direction of the magnetic field in the presence of strong magnetic field. The average Nusselt number decreases with an increase of the Hartmann number and increases with increase of the Grashof number and aspect ratio.

Key words: *Natural Convection; Magnetic field; Partially active walls; Finite volume method; Enclosure.*

1. Introduction

Natural convection in rectangular enclosures with partially heated or partially cooled vertical walls while the other two walls are kept adiabatic is of special interest in many engineering applications such as solar receivers, solar passive design and cooling of electronic equipment. A detailed study of the convective flow and heat transfer in a partially heated/cooled enclosure is very helpful to understand the complex phenomena of natural convection in practical applications. Kuhn and Oosthuizen [1] numerically studied unsteady natural convection in a partially heated rectangular enclosure. They found that the average Nusselt number increases to maximum and then decreases when the heater location moves from the top to bottom. Tanda [2] numerically analyzed laminar natural convection of air in open vertical channels with partially heated walls. In this study, both uniform wall

temperature and uniform heat flux boundary conditions are studied. Valencia and Frederick [3] studied natural convection of air in a square cavity with half-active and half-insulated vertical walls. They considered five different thermally active locations. Natural convection in a rectangular enclosure with four discrete heaters is investigated numerically and experimentally by Ho and Chang [4].

Convective flow in a partially heated and partially cooled cavity is numerically analyzed by Yucel and Turkoglu [5]. They observed that the mean Nusselt number decreases with increasing the heater size for a given cooler size. On the other hand, the mean Nusselt number increases with increasing the cooler size for a given heater size. Numerical simulations of laminar natural convection in a partially cooled differentially heated cavity are performed by El-Refaee *et al*. [6]. They found that the rate of heat transfer reaches its maximum value when the cavity is vertical with aspect ratio unity. Nithyadevi *et al*. [7] and Kandaswamy *et al*. [8] studied the natural convection in a square cavity with partially thermally active vertical walls. They considered nine different thermally active locations. Chen and Chen [9] numerically studied natural convection in a cavity with partially heated on the left and bottom walls. They found that the heat transfer rate is increased with increasing the length of the heat source. Oztop and Abu-Nada [10] numerically investigated convection of nanofluids in a partially heated rectangular enclosure. They found that the heater location influences on flow field and temperature distributions. Arici and Sahin [11] numerically investigated natural convection in a partially divided trapezoidal enclosure with summer and winter conditions. They found that the heat transfer results are not significantly altered by the presence of divider for summer condition.

Sivakumar *et al.* [12] numerically studied the mixed convection in a lid-driven cavity with different lengths and locations of the heater. They found that the heat transfer rate is enhanced when the location of heater is at middle or top on the left wall of the cavity. Natural convection flow inside a prismatic cavity has been numerically examined by Aich *et al*. [13]. They found that flow and temperature fields are strongly affected by the shape of the enclosure. Delavar *et al*. [14] investigated the effect of the heater location on flow pattern and heat transfer in a cavity using lattice Boltzmann method. The results show that higher heat transfer is observed from the cold walls when the heater located on vertical wall. Sivasankaran *et al*. [15] numerically studied the effect of discrete heating on natural convection in a porous enclosure. They concluded that the heat transfer rate is high at both heaters for smaller heater length ratio. Recently, Sankar *et al*. [16] numerically investigated natural convection in a porous cavity with partially thermally active walls. Terekhov *et al*. [17] made a numerical simulation on buoyant convection in a square enclosure with multiple partitions. Their result shows that the Nusselt number increases significantly with an increase in heat conductivity coefficient of partitions. Bhuvaneswari *et al*. [18] numerically analyzed the effect of aspect ratio on convection in a rectangular cavity with partially thermally active walls. They found that the heat transfer rate is decreased on increasing the aspect ratio.

Convective heat transfer in the presence of a magnetic field have been used extensively in many applications such as crystal growth, geothermal reservoir, metallurgical applications involving casting and solidification of metal alloys. Rudraiah *et al*. [19] numerically investigated the effect of the magnetic field on natural convection in a

rectangular enclosure. They found that the rate of heat transfer decreases in the presence the magnetic field. Khanafer and Chamkha [20] numerically studied hydromagnetic convection of a heat generating fluid in an inclined square porous cavity saturated with an electrically conducting fluid. They found that the heat transfer rate is reduced by the effect of the magnetic field. Qi *et al*. [21] studied natural convection in a cavity with partially heated from below in the presence of an imposed non-uniform magnetic field. They found that the velocity decreases with increasing the magnetic field strength. Hossain *et al*. [22] numerically investigated buoyancy and thermocapillary driven convection of an electrically conducting fluid in an enclosure with internal heat generation. They found that increase in the value of heat generation causes the development of more cells inside the cavity.

Natural convection of an electrically conducting fluid in a laterally and volumetrically heated square cavity under the influence of a magnetic field is investigated by Sarris *et al*. [23]. They concluded that the heat transfer is enhanced with increasing internal heat generation parameter, but no significant effect of the magnetic field is observed due to the small range of the Hartmann numbers. Sivasankaran and Ho [24] numerically analyzed the effects of temperature dependent properties on magneto convection in a cavity. They found that the heat transfer rate increases with increasing the Rayleigh number and decreases with increasing the Hartmann number. Double diffusive natural convection in trapezoidal porous cavity in the presence of transverse magnetic field has been studied numerically by Younsi [25]. He found that the overall heat and mass transfers decrease on increasing the magnetic field. Kolsi *et al*. [26] studied the effect of an external magnetic field on natural convection of liquid metals in a cubic cavity. They observed that the generated entropy is distributed on the entire cavity in the presence of a magnetic field.

Bhuvaneswari *et al*. [27] investigated magnetic convection in an enclosure with non-uniform heating on both walls. They found that the heat transfer rate is increased on increasing the amplitude ratio. Sivasankaran *et al*. [28] numerically examined the mixed convection in a square cavity with sinusoidal temperature on vertical walls in the presence of a magnetic field. They revealed that increasing the Hartmann number results in the decrease of the total heat transfer rate. Sivasankaran *et al*. [29] numerically studied the MHD convection of cold water in an open cavity with variable fluid properties. They observed that convection is enhanced by thermo-capillary force when buoyancy force is weakened. The effect of partition on magneto convection in a cavity is investigated by Sivasankaran *et al*. [30]. They found that the heat transfer rate with a horizontal partition is lower than with a vertical partition for given Hartmann and Grashof numbers.

To best of our knowledge, natural convection in enclosures with partially active vertical walls in the presence of magnetic field has received less attention in literature. Therefore, the main objective of the present study is to analyze the effect of the magnetic field and aspect ratio on convective flow and heat transfer in a rectangular enclosure with partially thermally active vertical walls.

2. Mathematical formulation

The physical configuration under consideration is a two-dimensional rectangular enclosure of length L and height H filled with an electrically conducting fluid as shown in Fig. 1. A portion of the left wall is kept at a constant temperature θ_h and a portion of the right wall is at temperature θ_c, with $\theta_h > \theta_c$. The remaining portions in the vertical walls and horizontal walls of the enclosure are insulated. Nine different thermally active locations will be studied here. That is, the hot region is located at the top, middle and bottom and the cold region is moving from bottom to top of their respective walls. It is also assumed that the uniform magnetic field $\boldsymbol{B} = B_x\boldsymbol{e}_x + B_y\boldsymbol{e}_y$ of constant magnitude $B_o = \sqrt{(B_x^2 + B_y^2)}$ is applied, where $\mathbf{e}_x$ and $\mathbf{e}_y$ are unit vectors in the Cartesian coordinate system. The orientation of the magnetic field form an angle ϕ with horizontal axis such that $\tan\phi = B_x / B_y$. The electric current $\boldsymbol{J}$ and the electromagnetic force $\boldsymbol{F}$ are defined by $\boldsymbol{J} = \sigma_e(\boldsymbol{V}\times\boldsymbol{B})$ and $\boldsymbol{F} = \sigma_e(\boldsymbol{V}\times\boldsymbol{B})\times\boldsymbol{B}$ respectively. The density of the fluid is assumed to be constant inside the enclosure except in the buoyancy term, in which it is taken as a function of the temperature through the Boussinesq approximation, $\rho = \rho_0[1-\beta(\theta-\theta_0)]$, where β being the coefficient of thermal expansion and subscript 0 denotes the reference state. The following assumptions are taken for this study. The fluid properties are constant. The flow is two-dimensional, laminar and incompressible. The radiation, viscous dissipation, induced electric current and Joule heating are neglected. The magnetic Reynolds number is assumed to be small so that the induced magnetic field can be neglected compared to the applied magnetic field.

The flow of laminar, incompressible, viscous fluid under the above specified geometrical and physical condition is governed by the following equations:

$$\frac{\partial u}{\partial x} + \frac{\partial v}{\partial y} = 0 \tag{1}$$

$$\frac{\partial u}{\partial t} + u\frac{\partial u}{\partial x} + \mathrm{v}\frac{\partial u}{\partial y} = -\frac{1}{\rho_0}\frac{\partial p}{\partial x} + \nu\left(\frac{\partial^2 u}{\partial x^2} + \frac{\partial^2 u}{\partial y^2}\right) - g\beta(\theta-\theta_0) + \frac{\sigma_e B_0^2}{\rho_0}(v\sin\phi\cos\phi - u\cos^2\phi) \tag{2}$$

$$\frac{\partial \mathrm{v}}{\partial t} + u\frac{\partial \mathrm{v}}{\partial x} + \mathrm{v}\frac{\partial \mathrm{v}}{\partial y} = -\frac{1}{\rho_0}\frac{\partial p}{\partial y} + \nu\left(\frac{\partial^2 \mathrm{v}}{\partial x^2} + \frac{\partial^2 \mathrm{v}}{\partial y^2}\right) + \frac{\sigma_e B_0^2}{\rho_0}(u\sin\phi\cos\phi - v\sin^2\phi) \tag{3}$$

$$\frac{\partial \theta}{\partial t} + u\frac{\partial \theta}{\partial x} + \mathrm{v}\frac{\partial \theta}{\partial y} = \alpha\left(\frac{\partial^2 \theta}{\partial x^2} + \frac{\partial^2 \theta}{\partial y^2}\right) \tag{4}$$

The appropriate initial and boundary conditions are:

$$\begin{aligned}
&t = 0: && u = \mathrm{v} = 0 && \theta = \theta_c\ , && 0 \le x \le H\ ,\ 0 \le y \le L \\
&t > 0: && u = \mathrm{v} = 0 && \frac{\partial \theta}{\partial x} = 0 && x = 0\ \&\ H \\
& && u = \mathrm{v} = 0 && \theta = \theta_h, && \text{heating portion} \quad y = 0 \\
& && u = \mathrm{v} = 0 && \theta = \theta_c, && \text{cooling portion} \quad y = L \\
& && && \frac{\partial \theta}{\partial y} = 0 && \text{elsewhere} \quad y = 0\ \&\ L
\end{aligned} \tag{5}$$

The following non-dimensional variables are used to non-dimensionalise the governing equations. $X = \frac{x}{L}$, $Y = \frac{y}{L}$, $U = \frac{u\,L}{\nu}$, $V = \frac{\mathrm{v}\,\mathrm{L}}{\nu}$, $T = \frac{\theta-\theta_c}{\theta_h-\theta_c}$, $\tau = \frac{t\ \nu}{L^2}$,

$\Psi = \frac{\psi}{\nu}$ and $\zeta = \frac{\omega L^2}{\nu}$. After eliminating the pressure terms, we get the vorticity-stream function formulation of the above equations (1) - (4) as follows,

$$\frac{\partial \zeta}{\partial \tau} + U\frac{\partial \zeta}{\partial X} + V\frac{\partial \zeta}{\partial Y} = \nabla^2 \zeta + Gr\frac{\partial T}{\partial Y} + Ha^2\left[\sin\phi\cos\phi\left(\frac{\partial V}{\partial Y} - \frac{\partial U}{\partial X}\right) + \left(\sin^2\phi\frac{\partial V}{\partial X} - \cos^2\phi\frac{\partial U}{\partial Y}\right)\right] \quad (6)$$

$$\nabla^2 \Psi = \zeta \quad (7)$$

$$\mathrm{U} = -\frac{\partial \Psi}{\partial Y},\ \mathrm{V} = \frac{\partial \Psi}{\partial \mathrm{X}} \text{ and } \zeta = \frac{\partial U}{\partial Y} - \frac{\partial V}{\partial X} \quad (8)$$

$$\frac{\partial T}{\partial \tau} + U\frac{\partial T}{\partial X} + V\frac{\partial T}{\partial Y} = \frac{1}{\mathrm{Pr}}\nabla^2 T \quad (9)$$

The initial and boundary conditions in the dimensionless form are:

$\tau = 0$; $U = V = \Psi = 0$, $\zeta = T = 0$, $0 \le X \le \mathrm{Ar}$, $0 \le Y \le 1$

$\tau > 0$: $U = V = \Psi = 0$, $\zeta = -\frac{\partial^2 \Psi}{\partial X^2}$, $\frac{\partial T}{\partial X} = 0$ $X = 0$ & Ar

$U = V = \Psi = 0$, $\zeta = -\frac{\partial^2 \Psi}{\partial Y^2}$, $T = 1$, heating portion, $Y = 0$ (10)

$U = V = \Psi = 0$, $\zeta = -\frac{\partial^2 \Psi}{\partial Y^2}$, $T = 0$, cooling portion, $Y = 1$

$U = V = \Psi = 0$, $\zeta = -\frac{\partial^2 \Psi}{\partial Y^2}$, $\frac{\partial T}{\partial Y} = 0$, elsewhere, $Y = 0$ & 1

The non-dimensional parameters that appear in the equations are the aspect ratio $\mathrm{Ar} = \frac{H}{L}$, Grashof number $Gr = \frac{g\beta(\theta_h - \theta_c)L^3}{\nu^2}$, Hartmann number $Ha = \frac{B_o^2 L^2 \sigma_e}{\mu}$ and Prandtl number $Pr = \frac{\nu}{\alpha}$. The heat transfer rate across the enclosure is an important parameter in thermal engineering applications. The local Nusselt number is defined by $Nu = -\left.\frac{\partial T}{\partial Y}\right|_{Y=0}$ resulting in the averaged Nusselt number as $\overline{Nu} = \frac{2}{Ar}\int_h NudX$ where *h=H/2* is the height of the heating location.

3. Method of solution

The non-dimensional governing equations (6) - (9) subject to the boundary conditions (10) are discretized using the finite volume method [31]. The power law scheme is used for the convection and diffusion terms. The implicit scheme is used for time marching. The solution domain consist a finite number of grid points at which the discretization equations are applied. The region of interest is covered with *m* vertical and *n* horizontal uniformly spaced grid lines in *X*- and *Y*-directions. The overall Nusselt number is used to develop an

understanding of what grid fineness is necessary for accurate numerical simulations. The grid sizes are tested from 41×41 to 121×121 for Ra=10^6 and *Pr*=0.054. It is observed from the grid independence test that a 81×81 uniform grid is enough to investigate the problem. At each time step the temperature and vorticity distributions are obtained from equations (9) and (6) respectively. The stream function distribution is obtained from equation (7) by using the Successive Over Relaxation (SOR) method and a known vorticity distribution. The boundary vorticity at solid walls can be obtained from the relation

$$\zeta_w = \frac{\Psi_{w+2} - 8\Psi_{w+1}}{2(\Delta h)^2} + O((\Delta h)^2), \tag{11}$$

where the subscript *w* denotes the boundary node. The velocities are then calculated using the stream function values. Finally, the numerical integration of the average Nusselt number is calculated by the Trapezoidal rule. The above process is repeated in the next time step until the steady state is reached. An iterative process is employed to find the stream function, vorticity and temperature fields. The process is repeated until the following convergence criterion satisfied for all variables (T, ζ, Ψ),

$$\left| \frac{\varphi_{n+1}(i, j) - \varphi_n(i, j)}{\varphi_{n+1}(i, j)} \right| \leq 10^{-5}. \tag{12}$$

Here *i* and *j* denote the grid points in *X*- and *Y*-directions respectively. The subscript *n* denotes the time step.

The validation of code is very important in computational studies. Therefore, the present computational code is verified against the existing results available in the literature. The quantitative results are compared with the corresponding solutions for natural convection in a square cavity [32, 33], natural convection in a cavity with partially active walls [3] and natural convection in the presence of the magnetic field [19]. They are shown in Tables 1, 2 and 3. It is observed from the tables that an agreement is obtained between the present results and previous results. An in-house code is used to simulate the present problem. The computations are carried out by computer with Intel core 2 Duo CPU and 2GB RAM.

4. Results and discussion

Numerical study is performed to understand the natural convection of an electrically conducting fluid in a rectangular enclosure with partially thermally active vertical walls in the presence of a uniform external magnetic field. It is clear that the non-dimensional parameters of interest are the aspect ratio (*Ar*), Grashof number (*Gr*), the Prandtl number (*Pr*), the Hartmann number (*Ha*), and the direction of the external magnetic field (ϕ). The value of the Prandtl number is chosen to be 0.054, corresponding to liquid metal in the present study. Computations are carried out for nine different thermally active locations with the Grashof numbers ranging from 10^3 to 10^6, the Hartmann numbers ranging from 10 to 100 and the aspect ratio from *Ar*=0.5 to 4. The direction of the external magnetic field with the horizontal axis is varying from ϕ=0° to 90°.

The flow pattern of the Middle-Middle heating location for *Ha*=10, 25 and 100, ϕ=0°, 45°, 90° and *Gr*=10^5 is shown in Figures 2(a-i). At ϕ=0° and *Ha*=10, the flow consists a single cell rotates clockwise direction and occupies the whole cavity, Fig. 2(a). When

increasing the angle to ϕ=45° or 90° there is no considerable change in the flow pattern for weak magnetic field. It is interesting to note that the cell elongated horizontally when increasing the Hartmann number to 25. When changing the angle of external magnetic field, there exists a small change in flow pattern for moderate magnetic field. Further increasing the Hartmann number to *Ha*=100, the flow pattern is affected very much by the orientation of the magnetic field. When ϕ=0° the flow has a vertical unicellular pattern, Fig. 2(g). The eddy is skewed elliptically towards the right-bottom and the left-top corners when ϕ=45°, Fig. 2(h). From the Fig. 2(i), the central streamlines are elongated horizontally and two secondary cells appear inside it as ϕ increases (ϕ=90°). The influence of a magnetic field on flow pattern is apparent from these figures. This is due to the retarding effect of the Lorentz force.

The isotherms of the Middle-Middle heating location for *Ha*=10, 25, 100, ϕ=0°, 45°, 90° and $Gr=10^5$ are shown in fig. 3(a-i). For weak magnetic field strength (*Ha*=10), there is a temperature stratification in the vertical direction and the thermal boundary layer is formed along the heating locations, which is clearly seen from the Fig. 3(a-c). It can be seen from these figures that convection is a dominant heat transfer mechanism. Increasing the Hartmann number to 25, there is a small noticeable change found in temperature field. Further increasing the Hartmann number (*Ha*=100), the vertical temperature stratification inside the cavity disappears and the thickness of the thermal boundary layers along the thermally active locations is reduced. This shows that convection is suppressed for all values of ϕ due to the strong magnetic field effect and hence the heat transfer in the cavity is mostly by conduction.

The streamlines for the Top-Bottom thermally active location with different directions of external magnetic filed, *Ha*=25 and $Gr=10^5$ are displayed in Fig. 4(a-c). The flow consists of a single cell with two inner cells and the centers of the inner cells are located near the thermally active parts of side walls as seen in Fig. 4 for all ϕ=0°, 45°, 90°. The position of the inner cells is changed by increasing the value of ϕ. The formation of such flow pattern reduces the heat transfer rate. The corresponding isotherms are plotted in Fig. 4(d-f). Figures 5(a-f) show the streamlines and isotherms for the Bottom-Top thermally active location with different directions of the external magnetic field, *Ha*=25 and $Gr=10^5$. The isotherms are crowded near the active locations on the right-bottom and the left-top corner of the cavity and form the thermal boundary layer. It is observed from this configuration that convection is dominated heat transfer mode. The streamlines and isotherms show almost similar pattern as like in Figs. 2-5. That is, there is no noticeable change on flow filed when changing the cooling location for a fixed heating location. However, a small change is observed in the temperature distribution near the thermally active location when changing the cooling location for a fixed heating location.

Figure 6 shows the mid-height velocity profiles for different thermally active locations, Hartmann numbers, ϕ=0° and $Gr=10^5$. The velocity of the particle is decreased with increasing the Hartmann number. The strong magnetic field decreases the flow speed inside the enclosure. The velocity of the fluid is higher in the Bottom-Top location whereas the velocity of the fluid is low in the Top-Bottom location. The local Nusselt number for different directions of the external magnetic field, Hartmann numbers and three active locations are depicted in Fig. 7(a-c). When changing the direction of the external magnetic field, a small variation in local Nusselt number is observed. Comparing these figures, it is observed that the

Middle-Middle location provides the higher local heat transfer rate. The value of local Nusselt number decreases along with the heater. The local Nusselt number slightly increases at the end of the heater when heat is at middle or bottom of the wall. Further scrutinizing these figures, local Nusselt number is reduced in the presence of magnetic field.

An important quantity of practical interest in the heat transfer analysis is the average heat transfer rate dissipated from the heating location and is measured from the dimensionless parameter average Nusselt number. In order to find the effect of thermally active location on magneto convection, the average Nusselt number is plotted for different heating and cooling locations along the vertical walls of the cavity in Fig. 8. It reveals clearly the effect of different thermally active locations on average heat transfer rate. It is observed that the heat transfer rate is enhanced in the Bottom-Top thermally active location and the heat transfer rate is poor in the Top-Bottom location. This is due to the buoyancy effect acts more effectively in the Bottom-Top location than that in the Top-Bottom location where the buoyancy is suppressed by horizontal wall in the Top-Bottom location.

In order to study the effect of the direction and strength of the external magnetic field on natural convection, the average Nusselt number is plotted as a function of the Hartmann and Grashof numbers for different values of ϕ in Figs. 9-11. It can be seen from the figure that there is a small change in the average heat transfer rate when changing the direction of external magnetic field. Among these three directions, ϕ=90° produces higher heat transfer rate for most thermally active locations. It is observed that the heat transfer rate decreases with increase in the Hartmann number for all directions of the external magnetic field and thermally active locations. It is observed that increasing the Grashof number increases the heat transfer rate. Fig. 12(a-c) show the effect of the aspect ratio against the average Nusselt number for different thermally active locations, different magnetic field strengths and directions and $Gr=10^5$. It is observed from the figures that the average Nusselt number increases with aspect ratio. It is also found that the rate of heat transfer is suppressed for high values of the Hartmann number.

5. Conclusions

The effect of orientation of the external magnetic field and partially thermally active zones on natural convection in an enclosure is studied numerically. The following are concluded from the study.

- The thermally active locations make great impact on convective flow and heat transfer. The Bottom-Top thermally active location gives higher heat transfer rate whereas the Top-Bottom location gives very poor heat transfer rate.
- Convective heat transfer is enhanced when heating location is either at the middle or bottom of the left wall while the cooling location is either at the top or middle of the right wall.
- The heat transfer rate decreases on increasing the strength of the magnetic field.
- The heat transfer rate increases on increasing the Grashof number and aspect ratio.
- The flow field is altered by changing the direction of external magnetic field in the presence of the strong magnetic field.

Nomenclature

Ar	Aspect ratio [-]
$\boldsymbol{B}$	magnetic field [T]
B_o	magnitude of the magnetic field [-]
$\boldsymbol{F}$	electromagnetic force [Nm^3]
$\boldsymbol{g}$	acceleration due to gravity [ms^{-2}]
Gr	Grashof number [-]
H	height of the enclosure [m]
Ha	Hartmann number [-]
$\boldsymbol{J}$	electric current [A]
L	length of the enclosure [m]
Nu	local Nesselt number ($=-\partial T/\partial Y$), [-]
$\overline{Nu}$	average Nusselt number [-]
P	pressure [Pa]
Pr	Prandtl number [-]
t	dimensional time [s]
T	dimensionless temperature ($=(\theta-\theta_c)/(\theta_h-\theta_c)$), [-]
u, v	velocity components [ms^{-1}]
U, V	dimensionless velocity components (=(u,v)L/ν), [-]
x, y	dimensional coordinates [m]
X, Y	dimensionless coordinates (=(x,y)/L), [-]

Greek Symbols

α	thermal diffusivity [m^2s^{-1}]
β	coefficient of thermal expansion [K^{-1}]
ζ	dimensionless vorticity (=ωL^2/ν), [-]
θ	temperature [K]
μ	dynamic viscosity [Nsm^{-2}]
ν	kinematic viscosity [m^2s^{-1}]
ρ	density [kgm^{-3}]
σ_e	electrical conductivity of the medium [S]
τ	dimensionless time (=tν/L^2), [-]
ϕ	direction of the external magnetic field [rad]
ψ	stream function [m^2s^{-1}]
Ψ	dimensionless stream function (=ψ/ν), [-]
ω	vorticity [s^{-1}]

Subscripts

c	cold wall
h	hot wall
0	reference state
w	conditions at wall/boundary

References

[1] Kuhn, D., Oosthuizen, P.H., Unsteady natural convection in a partially hearted rectangular enclosure, *Journal of Heat Transfer*, 109 (1987), pp. 798 - 801

[2] Tanda, G., Natural convection in partially heated vertical channels, *Heat and Mass Transfer*, 23 (1988), pp. 307-312

[3] Valencia, A., Frederick, R. L., Heat transfer in square cavities with partially active vertical walls, *International Journal of Heat and Mass Transfer*, 32 (1989), pp. 1567-1574

[4] Ho, C. J., Chang, J. Y., A study of natural convection heat transfer in a vertical rectangular enclosure with two-dimensional discrete heating: Effect of aspect ratio, *International Journal of Heat and Mass Transfer*, 37 (1994), 6, pp. 917 - 925

[5] Yucel, N., Turkoglu, H., Natural convection in rectangular enclosures with partial heating and cooling, *Heat and Mass Transfer*, 29 (1994), pp. 471 - 478

[6] El-Refaee, M.M., Elsayed, M.M., Al-Najem, N.M., Noor, A.A., Natural convection in partially cooled tilted cavities, *International Journal of Numerical Methods in Fluids*, 28 (1998), pp. 477 - 499

[7] Nithyadevi, N., Kandaswamy, P., Sivasankaran, S., Natural Convection on a Square Cavity with Partially Active Vertical Walls: Time Periodic Boundary Condition, *Mathematical Problems in Engineering*, 2006 (2006), pp. 1 – 16

[8] Kandaswamy, P., Sivasankaran, S., Nithyadevi, N., Buoyancy-driven convection of water near its density maximum with partially active vertical walls, *International Journal of Heat and Mass Transfer*, 50 (2007), pp. 942 – 948

[9] Chen, T.H., Chen, L.Y., Study of buoyancy-induced flows subjected to partially heated sources on the left and bottom walls in a square enclosure, *International Journal of Thermal Sciences*, 46 (2007), pp. 1219-1231

[10] Oztop, H.F., Abu-Nada, E., Numerical study of natural convection in partially heated rectangular enclosures filled with nanofluids, *International Journal of Heat and Fluid Flow*, 29 (2008) pp. 1326-1336

[11] Arici, M.E., Sahin, B., Natural convection heat transfer in a partially divided trapezoidal enclosure, *Thermal Science*, 13(4) (2009), pp. 213 - 220

[12] Sivakumar, V., Sivasankaran, S ., Prakash, P., Lee, J., Effect of heating location and size on mixed convection in lid-driven cavity, *Computers & Mathematics with Applications*, 59 (2010), pp. 3053-3065.

[13] Aich, W., Hajri, I., Omri, A., Numerical analysis of natural convection in a prismatic enclosure, *Thermal Science*, 15(2) (2011), pp. 437-446

[14] Delavar, M.A., Farhadi, M., Sedighi, K., Effect of discrete heater at the vertical wall of the cavity over the heat transfer and entropy generation using lattice Boltzmann method, *Thermal Science*, 15(2) (2011), pp. 423-435

[15] Sivasankaran, S., Do, Y., Sankar, M., Effect of Discrete Heating on Natural Convection in a Rectangular Porous Enclosure, *Transport in Porous Media*, 86 (2011), 291–311

[16] Sankar, M., Bhuvaneswari, M., Sivasankaran, S., Do, Y., Buoyancy Induced Convection in a Porous Enclosure with Partially Active Thermal Walls, *International Journal of Heat and Mass Transfer*, 54 (2011) pp. 5173-5182

[17] Terekhov, V.I., Chichindaev, A.V., Ekaid, A.l., Buoyancy heat transfer in staggered dividing square enclosure, *Thermal Science*, 15(2) (2011), pp. 409 - 422

[18] Bhuvaneswari, M., Sivasankaran S., Kim, Y.J., Effect of aspect ratio on convection in a porous enclosure with partially active thermal walls, *Computers & Mathematics with Applications*, (2011), in press (doi:10.1016/j.camwa.2011.09.033)

[19] Rudraiah, N., Barron, R.M., Venkatachalappa, M., Subbaraya, C.K., Effect of a magnetic field on free convection in a rectangular enclosure, *International Journal of Engineering Science*, 33 (1995), 8, pp. 1075-1084

[20] Khanafer, K.M., Chamkha, A.J., Hydromagnetic natural convection from an inclined porous square enclosure with heat generation, *Numerical Heat transfer A*, 33 (1998), pp. 891 - 910

[21] Qi, J., Wakayama, N.I., Yabe, A., Attenuation of natural convection by magnetic force in electro-nonconducting fluids, *Journal of Crystal Growth*, 204 (1999), pp. 408 - 412

[22] Hossain, M.A, Hafiz, M.Z., Rees, D.A.S., Buoyancy and thermocapillary driven convection flow of an electrically conducting fluid in an enclosure with heat generation, *International Journal of Thermal Sciences*, 44, (2005), pp. 676 - 684

[23] Sarris, I.E., Kakarantzas, S.C., Grecos, A.P., Vlachos, N.S., MHD natural convection in a laterally and volumetrically heated square cavity, *International Journal of Heat and Mass Transfer*, 48 (2005), pp. 3443 – 3453

[24] Sivasankaran, S., Ho, C.J., Effect of temperature dependent properties on MHD convection of water near its density maximum in a square cavity, *International Journal of Thermal Sciences*, 47 (2008), pp. 1184–1194

[25] Younsi, R., Computational analysis of MHD flow, heat and mass transfer in trapezoidal porous cavity, *Thermal Science*, 13(1) (2009), pp. 13-22

[26] Kolsi, L., Abidi, A., Borjini, M.N., Aïssia, H.B., The effect of an external magnetic field on the entropy generation in three-dimensional natural convection, *Thermal Science*, 14(2) (2010), pp. 341-352

[27] Bhuvaneswari, M., Sivasankaran S., Kim, Y.J., Magneto-convection in an Enclosure with Sinusoidal Temperature Distributions on Both Side Walls, *Numerical Heat Transfer A*, 59 (2011), pp. 167-184

[28] Sivasankaran, S., Malleswaran, A., Lee, J., Sundar P., Hydro-magnetic combined convection in a lid-driven cavity with sinusoidal boundary conditions on both sidewalls, *International Journal of Heat and Mass Transfer*, 54 (2011), pp. 512-525

[29] Sivasankaran, S., Bhuvaneswari, M., Kim, Y.J., Ho, C.J., Pan, K.L., Magneto-convection of cold water near its density maximum in an open cavity with variable fluid properties, *International Journal of Heat and Fluid Flow*, 32 (2011), pp. 932-942

[30] Sivasankaran, S., Bhuvaneswari, M., Lee, J., Effect of the partition on hydro-magnetic convection in a partitioned enclosure, *Arabian Journal of Science & Engineering*, (2011), in press (doi:10.1007/s13369-011-0110-4)

[31] Patankar, S. V., Numerical heat transfer and fluid flow. Hemisphere, McGraw-Hill, Washington, DC., 1980

[32] Davis, G.D.V., Natural convection of air in a square cavity: A bench mark numerical solution, *International Journal of Numerical Methods for Fluids*, 3 (1983), pp. 249 - 264

[33] Emery, A.F., Lee, J.W., The effects of property variations on natural convection in a square enclosure, *Journal of Heat Transfer*, 121 (1999), pp. 57 – 62

Table 1. Comparison of average Nusselt number with previous works for square cavity with fully heated vertical walls

Pr	0.1		0.71				1.0	
Ra	10^4	10^5	10^3	10^4	10^5	10^6	10^4	10^5
Davis [32]	-	-	1.116	2.234	4.510	8.869	-	-
Emery & Lee [33]	2.011	3.794	-	-	-	-	2.226	4.500
Present	2.126	3.972	1.110	2.236	4.496	8.658	2.247	4.572

Table 2. Comparison of average Nusselt number with previous works for square cavity with partially heated walls

Ra	10^4			10^5			10^6		
Model	TB	MM	BT	TB	MM	BT	TB	MM	BT
Valencia & Frederick [3]	2.142	3.399	2.997	3.295	6.383	5.713	4.505	12.028	11.659
Present	2.089	3.318	2.888	3.136	6.198	5.643	4.397	11.532	10.982

TB $\rightarrow$ Top-Bottom; MM $\rightarrow$ Middle-Middle; BT $\rightarrow$ Bottom-Top

Table 3. Comparison of average Nusselt number with previous works for magnetic convection in a square cavity with $Gr=2\times10^5$

Ha	0	10	50	100
Rudraiah *et al.* [19]	4.9198	4.8053	2.8442	1.4317
Present	5.0025	4.8148	2.8331	1.4341

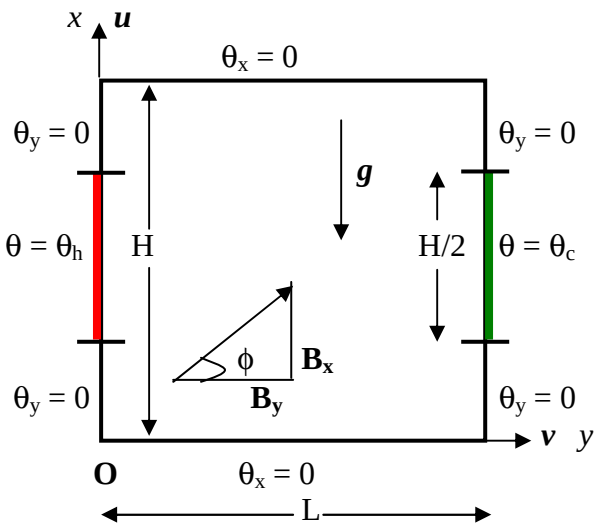

Figure 1 Physical configuration and boundary conditions

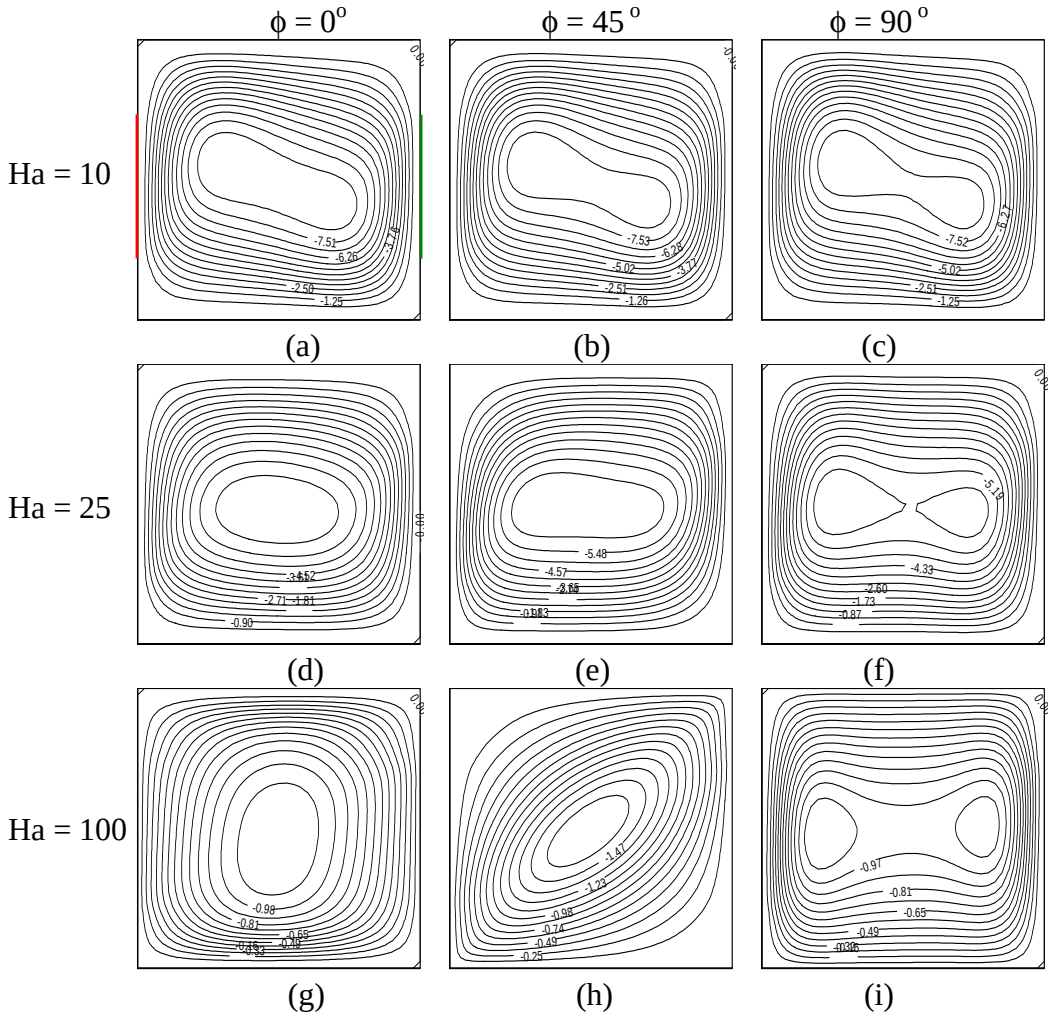

Figure 2 Streamlines of Middle-Middle location for different ϕ, different Ha and Gr=10^5.

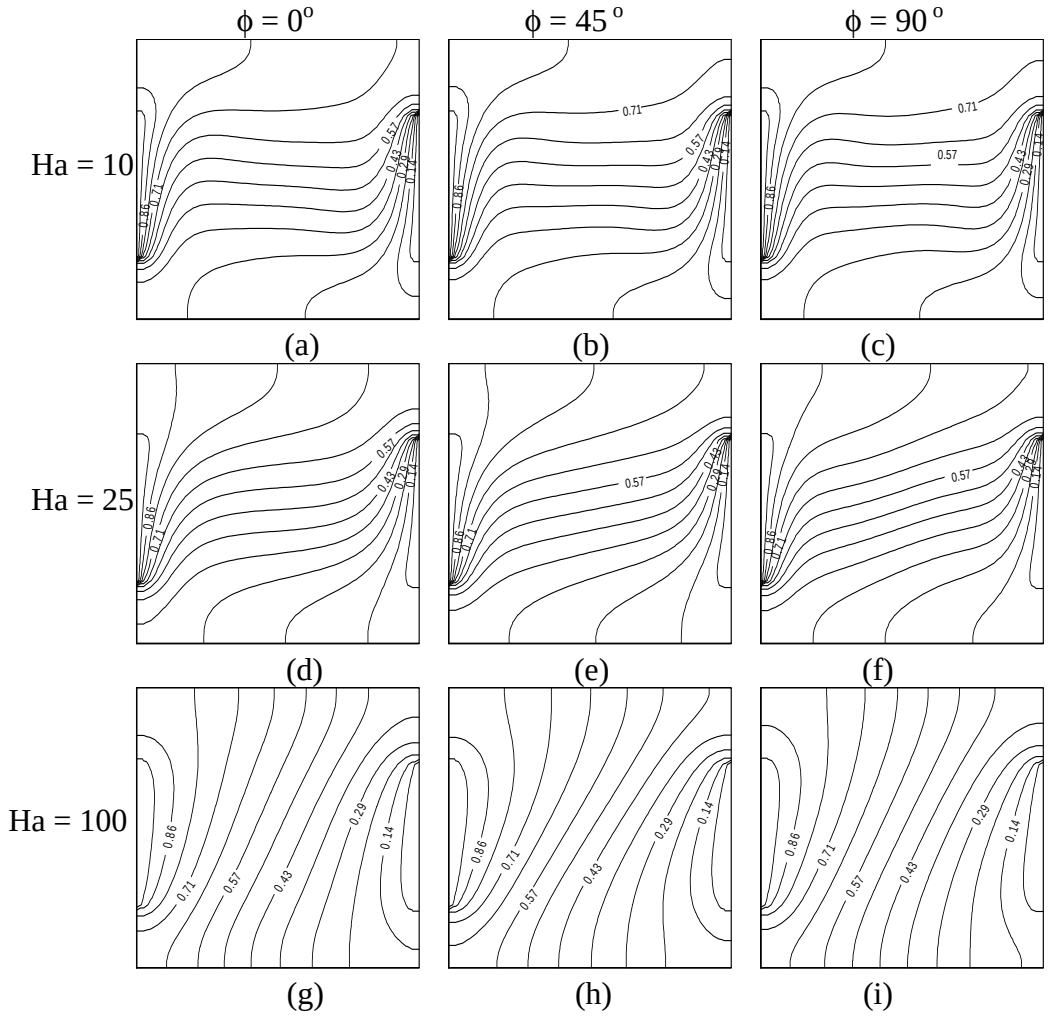

Figure 3 Isotherms of Middle-Middle location for different ϕ, different Ha and Gr = 10^5.

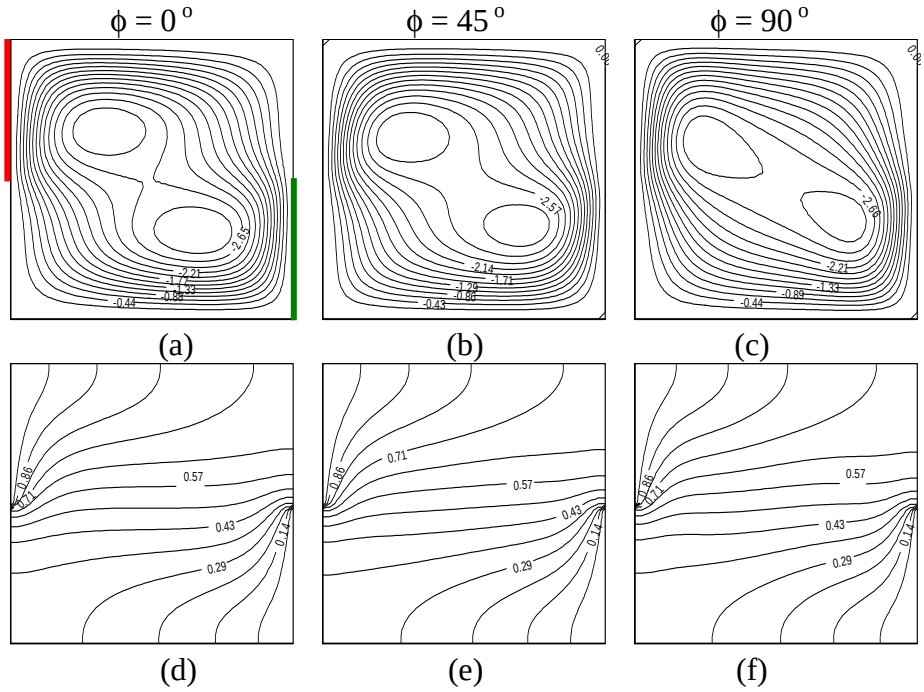

Figure 4 Streamlines and isotherms of Top-Bottom location for different ϕ, Ha = 25 and Gr = 10^5.

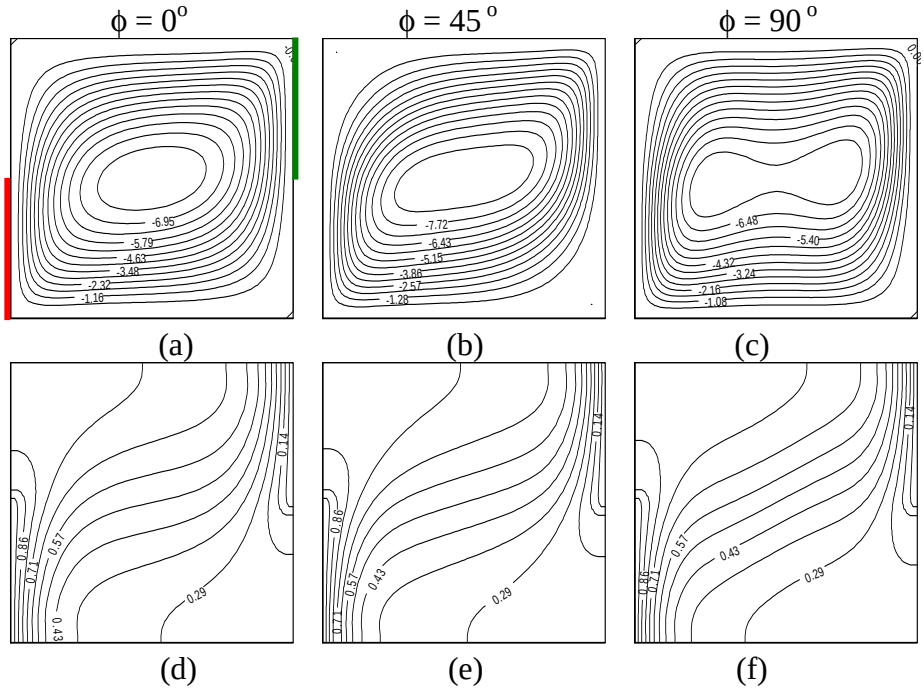

Figure 5 Streamlines and isotherms of Bottom-Top location for different ϕ, Ha = 25 and Gr = 10^5.

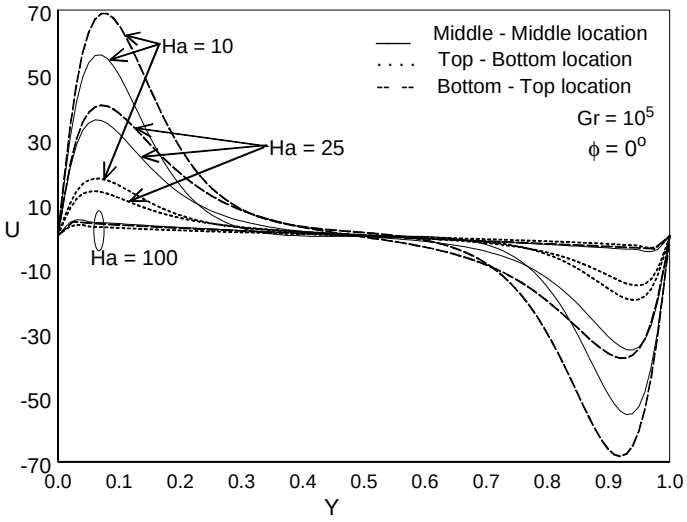

Figure 6 Mid-height velocity profiles for different Hartmann number

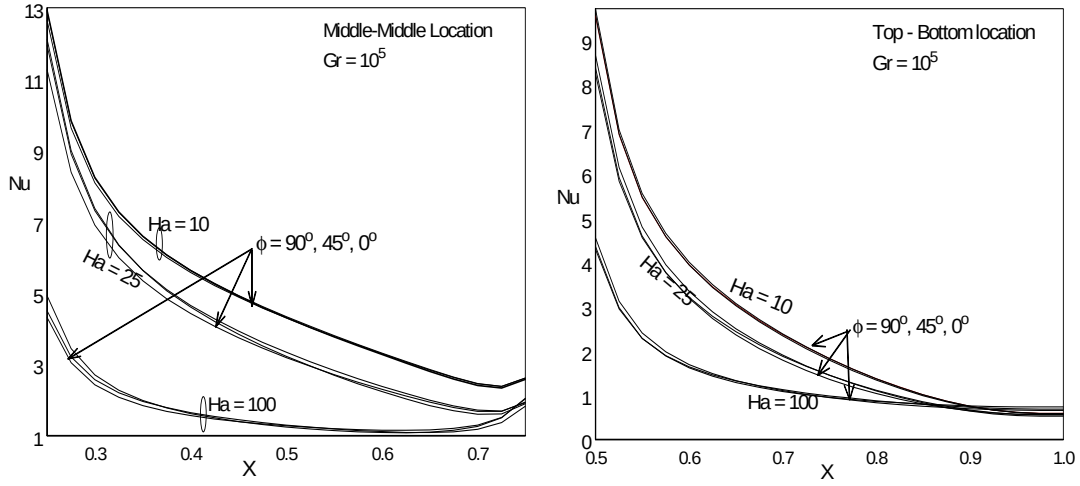

(a) Middle-Middle location (b) Top-Bottom location

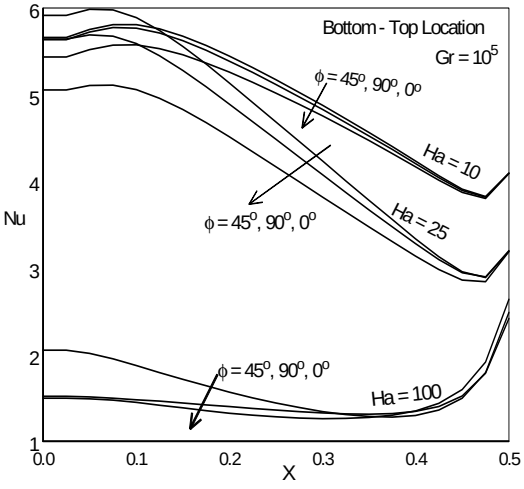

(c) Bottom-Top location

Figure 7 Local Nusselt number for different ϕ and Hartmann number

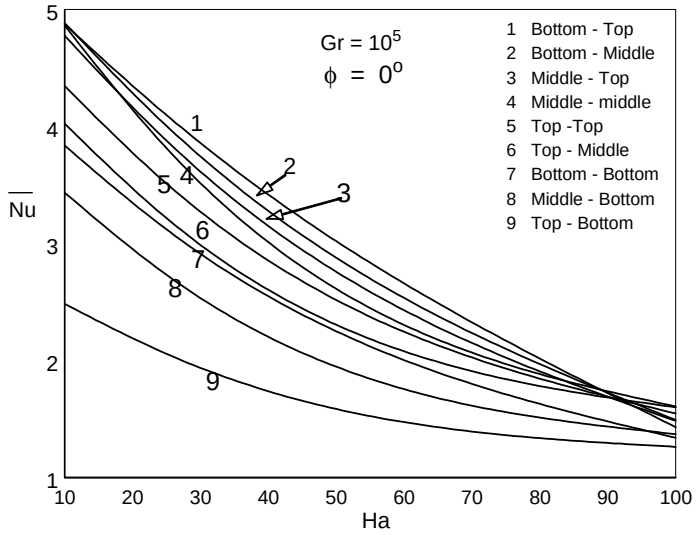

Figure 8 Average Nusselt number versus Hartmann number for different locations

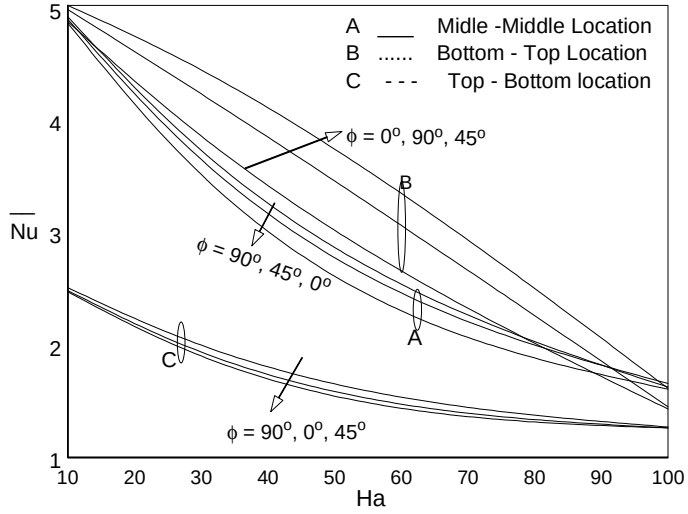

Figure 9 Average Nusselt number versus Hartmann number for different ϕ

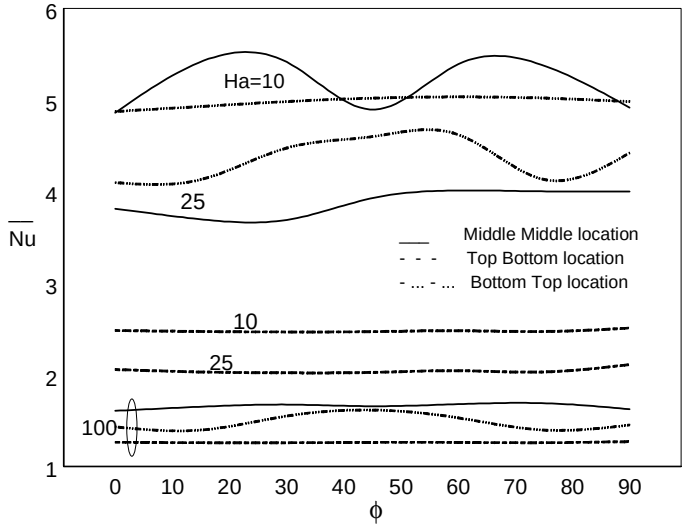

Figure 10 Average Nusselt number versus ϕ for different Hartmann numbers

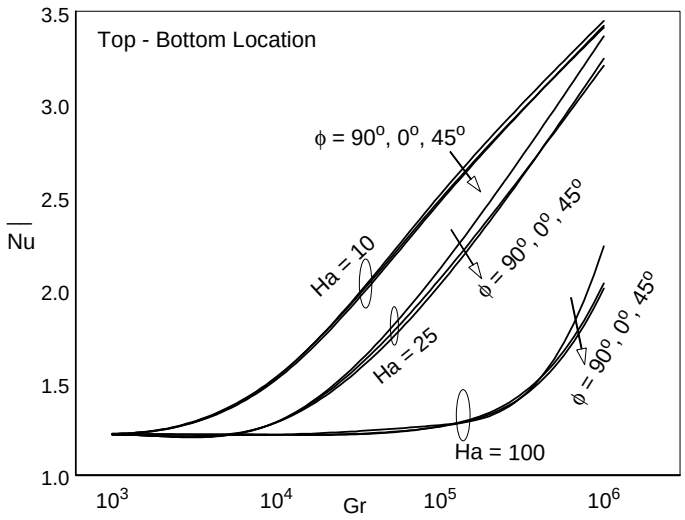

(a) Top–Bottom location

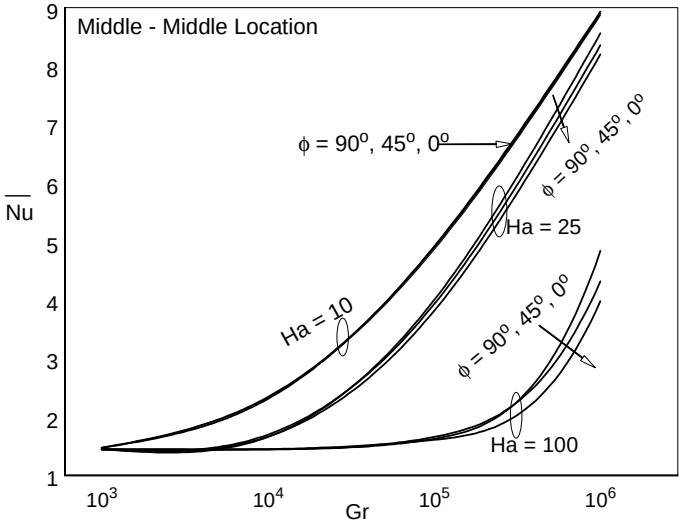

(b) Middle–Middle location

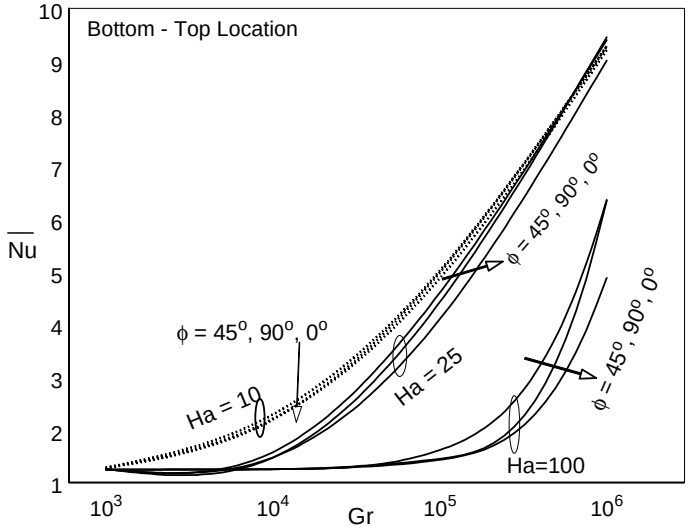

(c) Bottom–Top location

Figure 11 Average Nusselt number versus Grashof numbers for different ϕ and Ha.

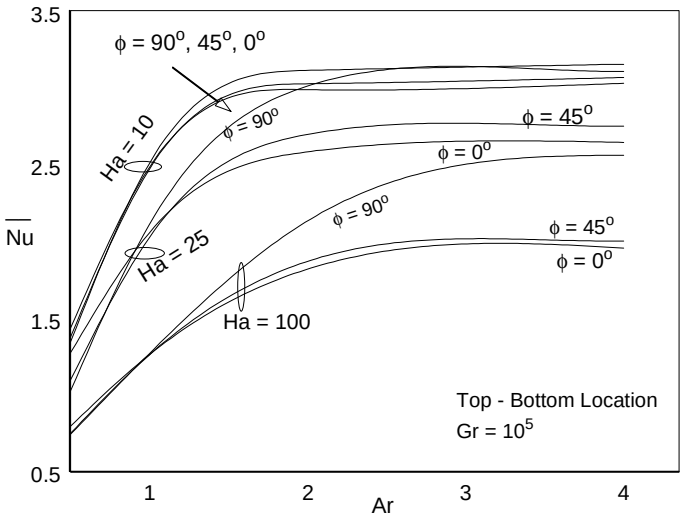

(a) Top–Bottom location

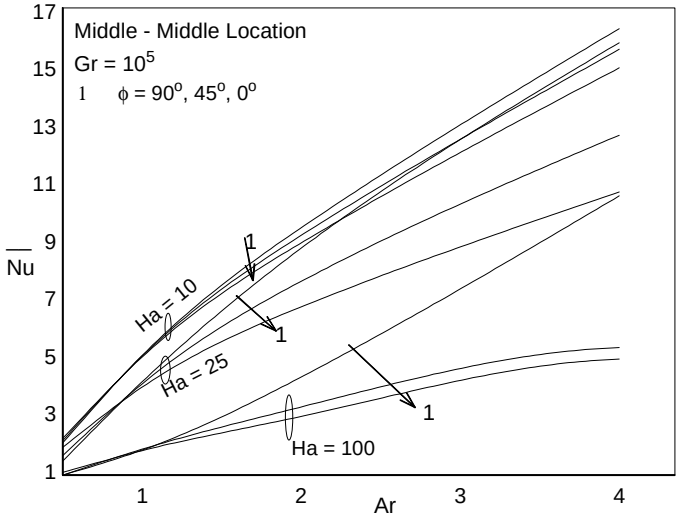

(b) Middle-Middle location

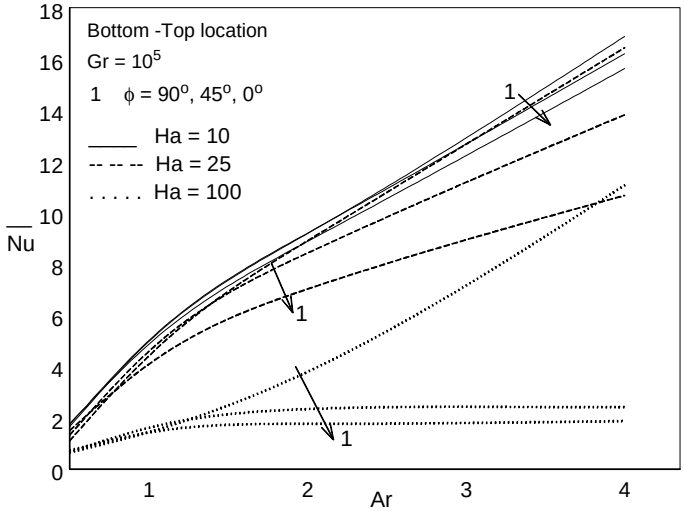

(c) Bottom-Top location

Figure 12 Average Nusselt number versus aspect ratio for different ϕ and Ha